Available online at www.sciencedirect.com
ScienceDirect
Journal of Solid State Chemistry 180 (2007) 2363–2370
JOURNAL OF SOLID STATE CHEMISTRY
www.elsevier.com/locate/jssc

Redetermination of the crystal structure of $Ge(HPO_4)_2 \cdot H_2O$, and its thermal behaviour in the range $300 \geqslant T \geqslant 16\,K$

Lars Peters*, John S.O. Evans

Department of Chemistry, University of Durham, Science Laboratories, South Road, Durham DH1 3LE, UK

Received 12 March 2007; received in revised form 4 June 2007; accepted 4 June 2007
Available online 16 June 2007

Abstract

The crystal structure of α-$Ge(HPO_4)_2 \cdot H_2O$ (α-GeP) was redetermined using X-ray powder diffraction methods. Reindexing the pattern showed that the monoclinic angle is $\beta = 108.985(1)^\circ$ and the lattice parameters $a = 8.2920(2)$ Å, $b = 4.7880(1)$ Å, $c = 16.4058(3)$ Å, rather than the reported $\beta = 110.2(4)^\circ$, $a = 8.230(2)$ Å, $b = 4.784(1)$ Å, $c = 16.502(5)$ Å in space group $P2_1/c$. This apparently minor change in the cell parameters is important as it otherwise leads to incorrect Ge–O and P–O distances. Variable temperature X-ray diffraction experiments give an insight into the thermal behaviour of α-GeP in the temperature range from 300 to 16 K. α-GeP behaves as expected for a layered structure, showing a much larger expansion perpendicular to the layers than within the layers. The monoclinic angle increases with decreasing temperature. No temperature induced phase transitions have been observed in the temperature interval studied.

Keywords: Layered compound; Chemical synthesis; Variable temperature X-ray diffraction

1. Introduction

α-$Ge(HPO_4)_2 \cdot H_2O$ (α-GeP) belongs to a family of materials known as *APTM* (acid phosphates of tetravalent metals), which have been of scientific interest for the last four decades. Several features of these substances have contributed to this interest, e.g., ion exchange [1,2], intercalation (e.g., [3,4]), proton conduction in inorganic materials [5] and catalysis [6]. Additionally, it is known that α-GeP can serve as a precursor material for the synthesis of the GeP_2O_7-polymorphs (e.g., [7]). Their γ-modification belongs to the MT_2O_7 family of substances, which is famous for an often observed thermal contraction behaviour (e.g., [8,9]). The very complex superstructure of γ-GeP_2O_7 is to date unknown. However, Losilla et al. [7] proposed a monoclinic or triclinic symmetry with at least 270 independent atoms in the asymmetric unit. Particularly because of this precursor function, the thermal behaviour of α-GeP above room temperature has been repeatedly studied using various techniques (e.g., [7,10,11]). The vibrational spectra of α-GeP have recently been reported [12]. Sub-ambient thermal expansion, however, has not yet been investigated. In order to obtain further insight into the structural properties of *APTM* and especially their thermal behaviour, the structure of $Ge(HPO_4)_2 \cdot H_2O$ was redetermined in this work. Part of the motivation came from a recent structure report [11] which stated some surprising Ge–O (between 1.44 and 2.38 Å) and P–O distances (1.45−2.03 Å) and intra-tetrahedral angles (69−136°) in the structure.

A brief introduction to general aspects of the α-$Zr(HPO_4)_2 \cdot H_2O$ structure type is given in Section 1.1. The synthesis and relevant experimental details are described in Section 2. The results of the experiments are presented and discussed in Section 3.

1.1. *The* α-$Zr(HPO_4)_2 \cdot H_2O$ (α-ZrP) *structure type*

Many hydrogenphosphate hydrates of tetravalent metals have the α-ZrP type structure. Evidence for the isotypy of the compounds with Si, Ge, Sn, Pb, Ti and Zr was first presented in [13]. The α-ZrP structure was first determined

*Corresponding author. Fax: +44 191 384 4737.
E-mail address: lars.peters@dur.ac.uk (L. Peters).

0022-4596/$ - see front matter © 2007 Elsevier Inc. All rights reserved.
doi:10.1016/j.jssc.2007.06.009

by Clearfield and Smith [14] from single crystal X-ray diffraction data. Since then, several other materials have been shown to be isotypic, for instance α-TiP (e.g., [15–17]), α-PbP and α-SnP [15]. However, a neutron powder diffraction study [16] suggested that the orientation of the water molecules may be subtly different in different materials. Such differences cannot, however, be resolved with X-ray powder diffraction techniques.

α-$Zr(HPO_4)_2 \cdot H_2O$ is monoclinic with space group $P2_1/c$, though the alternate setting $P2_1/n$ (with a smaller monoclinic angle) is frequently used in the literature (e.g., [18]). For α-SnP, a translationengleiche supergroup of index $t2$, $C2/c$, was chosen for the structure refinement [15], due to only small supercell reflection intensities being visible and hence only small deviations from the higher symmetry. For the sake of simplicity and direct comparability with the initial structural work by [11,14], the $P2_1/c$ setting and symmetry is used in this work.

A schematic drawing of the structure (protons omitted) is shown in Fig. 1 in a projection along the **b** axis. The *M* cations are located alternately above and below the **ab**-planes at $z = 0$ and $\frac{1}{2}$, and are sixfold coordinated by oxygen in the shape of an octahedron. The coordination polyhedron distorts slightly, depending on the species of *M* (e.g., [15,18]). The [MO_6] octahedron is all-corner connected to slightly distorted [PO_4] tetrahedra, forming layers of [MO_6] octahedra and [PO_4] tetrahedra. Only three corners of the two crystallographically unique tetrahedra participate in the formation of these layers, while the fourth corner is bonded to hydrogen, with the P–O bond vector almost normal to the **ab**-plane. Typically, the P–O(H) bond is about 1.6 Å, slightly longer than the other P–O bonds (≈ 1.51 Å). The arrangement of the layers leads to the formation of "zeolitic"-type cavities [14], which are occupied by one water molecule each, forming one intralayer hydrogen bond, while the other hydrogen points towards the bottom/top of the cavity and is not involved in hydrogen bonding. Both P–OH groups are involved in hydrogen bonds towards the water oxygen. According to [14,15,18], no inter-layer hydrogen bonds exist, implying that the layers are only linked by weak van der Waals interaction in the **c** direction.

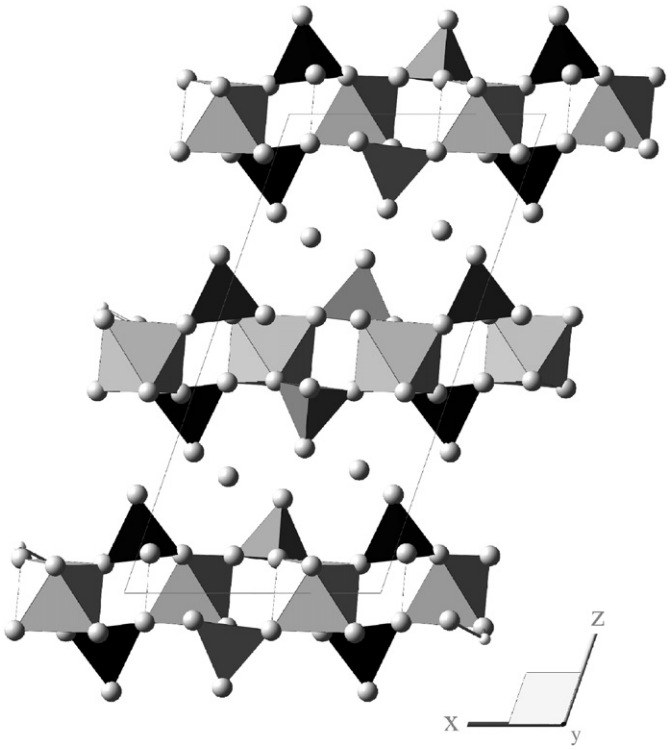

Fig. 1. Schematic view of the crystal structure of α-GeP along the [0 1 0]-direction. Spheres represent oxygen, light octahedra are [GeO_6]-coordination polyhedra, dark tetrahedra represent [$P1O_4$] and lighter tetrahedra [$P2O_4$]. Lone oxygens correspond to the interlayer water oxygen positions.

2. Experimental

2.1. Synthesis

α-GeP was synthesised, following essentially the route described by [7]. The 1.6944 g of amorphous GeO_2 (*Aldrich*, 99.99 + %) were dispersed in 11.66 g demineralised water. After homogenising, 37.42 g H_3PO_4 (85 wt% solution) were added under constant stirring. After leaving the suspension for four days (with regular stirring), it was sealed in a teflon-lined *Paar* autoclave at 125 °C for seven days. After washing several times with demineralised water and acetone, the obtained white material was centrifuged and dried at 60 °C. X-ray powder diffraction confirmed that the sample was single phase α-GeP.

2.2. Variable temperature X-ray powder diffraction

X-ray diffraction data were collected using a *Bruker-AXS D8* diffractometer equipped with a Cu tube and Ni-filter, giving Cu $K\alpha_1$ and Cu $K\alpha_2$ ($\lambda_1 = 1.540598$ Å, $\lambda_2 = 1.544426$ Å, respectively) radiation; data were recorded using a *LynxEye* semiconductor strip detector (SSD). The diffractometer was operated in Bragg–Brentano geometry, using ϑ/ϑ scans.

Samples were prepared by sprinkling finely ground powder onto a Vaseline-coated Al sample holder. The room temperature data set was collected in the 2ϑ-range 10–100°, using a step size of $\Delta 2\vartheta = 0.0057°$ and a counting time of 0.1 s/step, summing up to 26 min in total.

Variable-temperature X-ray data from 300 to 16 K were collected using an *Oxford Cryosystems pheniX* cryostat. The sample was prepared by sprinkling finely ground powder onto a zero background silicon wafer. The 20 min data collections were performed, in the 2ϑ-range 10–100° using a step size of $\Delta 2\vartheta = 0.01°$ and a counting time of 0.14 s/step, as the sample was cooled to 16 K. Data were thus collected in approximately 4 K steps. Mean temperatures for each range were extracted from readings taken at 30 s intervals during the measurements. Independent checks using a variety of well characterised materials suggest that temperatures quoted are accurate to 3 K.

Lattice and structural parameters were derived using the Pawley [19] and the Rietveld method [20] within the *TOPAS* suite of programs [21].

3. Results and discussion

3.1. Redetermination of the crystal structure of $Ge(HPO_4)_2 \cdot H_2O$

Initially, the structure for α-GeP as given by Romano et al. [11] was used as a model for refinement against the X-ray data collected at room temperature. Because of their low scattering power, the protons were left out of all structure refinements. The reflections of the sample holder (Al) were fitted simultaneously, using the Pawley method [19]. A background polynomial, peak shape parameters, and the sample height were refined. As a result of the preparation, a preferred orientation was observed for α-GeP, which was accounted for by a March–Dollase approach [22], yielding a significant plate-character along [0 0 1].

The refinement converged readily and gave a fit to the experimental data very similar to the published results [11], with $R_{wp}=18.7\%$, $R_p=13.2\%$, $R_{Bragg}=6.9\%$ and $GOF(\chi^2)=3.99$. The refined lattice parameters were: $a=8.283(1)$ Å, $b=4.790(1)$ Å, $c=16.523(1)$ Å, and $\beta=110.037(1)^\circ$. Whilst the fit to the experimental data looked reasonable at first glance, more careful examination showed significant systematic differences between observed and calculated patterns. In fact the differences appeared essentially identical to those in the Rietveld plot published by Romano et al. [11].

The pattern therefore was re-indexed using the *TOPAS* suite of programs [23]. The best agreement was found for a monoclinic cell in space group $P2_1/c$, but with a monoclinic angle of approximately 109°, rather than the published 110.2°. Subsequently, the cell here found, combined with the fractional coordinates for α-ZrP (single crystal data [14]), were used as a starting model. Fig. 2 shows a plot of the result of the refinement using the Rietveld method. The refined lattice parameters and final Rietveld statistics are: $a=8.2920(2)$ Å, $b=4.7880(1)$ Å, $c=16.4058(3)$ Å, $\beta=108.985(1)^\circ$, $R_{wp}=9.66\%$, $R_p=7.06\%$, $R_{Bragg}=3.67\%$ and $GOF(\chi^2)=2.07$.

The small but significant differences between the two cells lead to pronounced differences in the reflection positions. This is exemplified in Fig. 3 for the reflections (1 1 2) and (2 0 $\bar{4}$). The permutation of the two reflection positions results in a characteristic misfit and therefore, intensity difference curve, which can also be observed in the original work [11]. The resultant inaccurate intensity distribution in the affected reflection-groups leads to incorrect fractional coordinates and hence, a chemically implausible structure. Clearly, on using the initial cell, the refinement converges to a local minimum. This local minimum was avoided in the present case by reindexing the powder pattern.

Refined atomic coordinates for α-GeP in space group $P2_1/c$ are given in Table 1. Due to the low scattering power of oxygen soft restraints were introduced for polyhedral bond angles, and bond valence sum restraints for cations and oxygens of Ge–O–P linkages. We consider bond valence restraints less prescriptive than bond length restraints. In the final refinement cycle, angle restraints were removed. Additionally removing the bond valence sum restraints led to a slight overbonding of Ge, and small distortions of P–O (1.45(2)–1.63(2) Å) and Ge–O (1.79–1.96 Å) distances. Hence, bond valence soft restraints were retained. For the sake of comparability, refined coordinates for α-ZrP from single-crystal work [14] are given in italics below our values. Selected bond lengths and angles are quoted in Tables 2 and 3. The general features of the structure are identical to those described in Section 1.1.

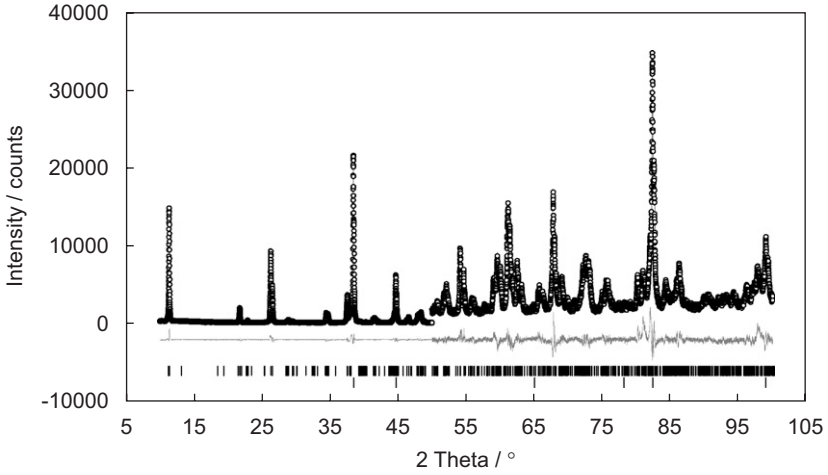

Fig. 2. Plot of the Rietveld refinement result of α-GeP at room temperature. Circles represent measured intensity and the solid line the calculated intensity. The difference curve is shown below. From $2\vartheta=50^\circ$, all intensities have been multiplied by 10. Vertical lines indicate the positions of the *Bragg*-reflections. Top row of tick-marks: α-GeP, bottom row: Al.

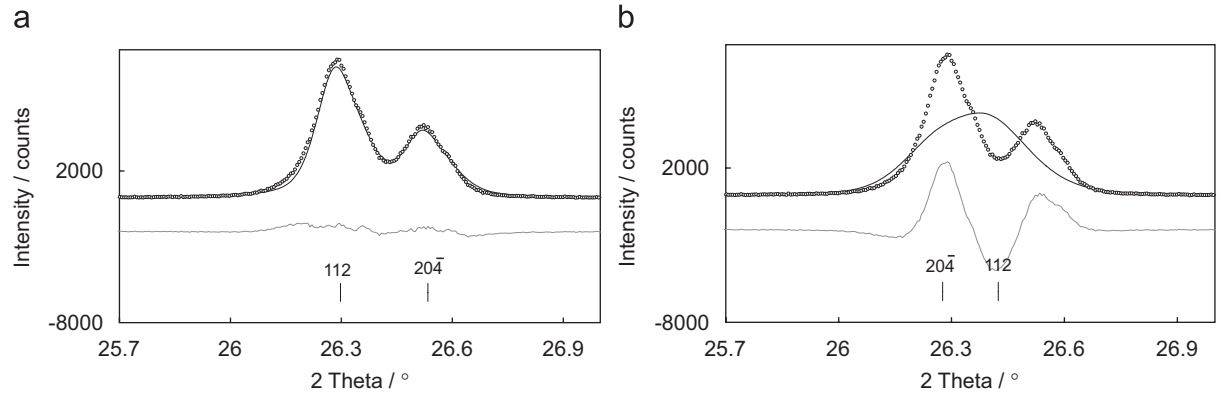

Fig. 3. Plot of one characteristic section of the Rietveld refinement, using (a) the re-determined cell and atomic coordinates reported here and (b) the reported structure for $Ge(HPO_4)_2 \cdot H_2O$ [11]. Both refinements converged with reasonable *R* values. Circles represent measured intensity and the solid line the calculated intensity; the difference curve is shown below. Vertical lines indicate the positions of the *Bragg*-reflections. The interchanged reflection positions result in the characteristic misfit and difference curve in (b).

Table 1
Refined structural parameters for α-GeP from X-ray powder diffraction data at room temperature in space group $P2_1/c$

Atom	*x/a*	*y/b*	*z/c*
Ge	0.7550(2)	0.2520(7)	0.5092(1)
Zr	*0.7606(2)*	*0.250(2)*	*0.5144(1)*
P1	−0.0077(2)	0.757(1)	0.6035(1)
	0.0008(6)	*0.752(5)*	*0.6129(4)*
P2	0.4676(3)	0.257(1)	0.0950(1)
	0.4711(6)	*0.255(5)*	*0.1044(4)*
O1	0.1212(6)	0.855(1)	0.5616(2)
	0.105(2)	*0.806(5)*	*0.560(1)*
O2	0.9469(6)	0.456(1)	0.5792(3)
	0.934(3)	*0.486(6)*	*0.601(2)*
O3	0.8310(6)	0.940(1)	0.5805(2)
	0.869(2)	*0.941(5)*	*0.589(4)*
O4	0.0821(6)	0.756(2)	0.7056(3)
	0.104(2)	*0.760(9)*	*0.716(1)*
O5	0.3077(6)	0.075(1)	0.0560(2)
	0.344(3)	*0.057(5)*	*0.062(1)*
O6	0.4372(6)	0.559(1)	0.0682(3)
	0.418(2)	*0.514(5)*	*0.069(1)*
O7	0.5085(6)	0.252(3)	0.1953(3)
	0.512(2)	*0.257(9)*	*0.205(1)*
O8	0.3747(6)	0.859(1)	0.9217(2)
	0.375(2)	*0.814(5)*	*0.910(1)*
O9	0.253(1)	0.276(2)	0.2586(4)
	0.254(2)	*0.265(8)*	*0.259(1)*

$a = 8.2930(2)$ Å, $b = 4.7885(1)$ Å, $c = 16.4092(2)$ Å, $\beta = 108.984(1)^\circ$, $B_{ov} = 0.03(2)$ Å^2. For comparison, refined coordinates for α-ZrP from single-crystal work [14] are given in italics below our values.

In agreement with the results of [14] for α-ZrP, Ge–O2 and Ge–O6 are the longest bonds (1.90(1) and 1.92(1) Å). The other Ge–O bonds are slightly shorter with values of 1.86(1)–1.88(1) Å. Since O2 and O6 are on opposite positions of the octahedron, the main distortion is a uniaxial elongation (O2–O6 is 3.82(1) Å, O1–O8 and O3–O5 are 3.72(1), 3.73(1) Å, respectively) towards a tetragonal bipyramid. The largest deviation from ideality in the intra-octahedra *cis* angles is 3° for the angle O2–Ge–O5, and 4.0° for the O3–Ge–O5 *trans* angle.

Both crystallographically unique $[PO_4]$ tetrahedra are distorted. In agreement with earlier findings, the P–O(H) bond is the longest bond in both crystallographically distinct tetrahedra: P1−O4 = 1.60(1) Å and P2−O7 = 1.57(1) Å. The average other P–O distances are 1.52 and 1.53 Å in $[P1O_4]$ and $[P2O_4]$, respectively. The largest deviation from ideality in the intra-tetrahedra angles is 4° for the angles O3–P1–O1 and O5–P2–O8, respectively. Significant distortion of the tetrahedra in α-GeP was recently assumed by Moraes et al. [12] due to the wide spread of $\nu_d(PO_3)$ modes in the Raman spectrum. However, the distortion of the tetrahedra in α-GeP is of the same order of magnitude as observed for α-ZrP [14].

Bruque et al. [15] concluded that in the series α-ZrP via α-TiP and α-SnP to α-PbP the "corrugation" of the layers increases. Corrugation here means that the metal atoms approach each other within the layers due to coupled polyhedral rotations, and "push" the phosphate groups into the interlayer space [15]; the P–O(H) vector becoming more closely perpendicular to the **ab**-plane as corrugation increases. The layered conformation of $[GeO_6]$ octahedra and $[PO_4]$ tetrahedra exhibits a stronger "corrugation" (comparable to α-PbP) than in α-ZrP. The driving force is probably the optimisation of the layer's fit to the interlayer water molecule. As the *M* site cation radius decreases, polyhedra undergo cooperative rotations which corrugate the structure and presumably optimise the hydrogen bonding interactions.

Bruque et al. [15] showed that the cell volume in α-ZrP type compounds correlates with the ionic radius of the tetravalent metal cation. They reported a linear relationship between the cell volume of the phases with Ti, Sn and Pb and their ionic radii, and discussed α-ZrP as being an anomaly, having too large a volume with respect to the observed trend. Including data for α-GeP from this work and α-HfP (from [16]) in this relationship, leads us to a different conclusion. As can be seen from Fig. 4(a–d), two

Table 2
Bond lengths in α-GeP in Å, derived from the structure refinement against the X-ray diffraction pattern at room temperature

Atom	O1	O2	O3	O4	O5	O6	O7	O8
Ge	1.86(1)	1.90(1)	1.88(1)		1.86(1)	1.92(1)		1.87(1)
P1	1.52(1)	1.51(1)	1.54(1)	1.60(1)				
P2					1.54(1)	1.51(1)	1.57(1)	1.53(1)
O9			3.12(1)	2.64(2)			2.65(1)	3.08(1)
				2.91(2)			2.95(2)	
				3.03(2)			3.13(2)	

Table 3
Bond angles in α-GeP in °, derived from the structure refinement against the X-ray diffraction pattern at room temperature

O–Ge–O	Value	O–P–O	Value	Ge–O–P	Value
O1–Ge–O5	89(1)	O1–P1–O2	109(1)	Ge–O1–P1	144(1)
O1–Ge–O6	88(1)	O1–P1–O4	109(1)	Ge–O2–P1	138(1)
O1–Ge–O3	92(1)	O2–P1–O3	111(1)	Ge–O3–P1	134(1)
O1–Ge–O8	179(1)	O3–P1–O4	109(1)	Ge–O5–P2	139(1)
O2–Ge–O1	90(1)	O3–P1–O1	113(1)	Ge–O6–P2	133(1)
O2–Ge–O5	87(1)	O4–P1–O2	106(1)	Ge–O8–P2	135(1)
O2–Ge–O3	89(1)				
O2–Ge–O8	92(1)				
O2–Ge–O6	176(1)				
O3–Ge–O8	89(1)	O5–P2–O7	107(1)		
O3–Ge–O6	94(1)	O5–P2–O6	112(1)		
O3–Ge–O5	176(1)	O5–P2–O8	113(1)		
O5–Ge–O6	90(1)	O6–P2–O8	112(1)		
O5–Ge–O8	91(1)	O7–P2–O8	106(1)		
O6–Ge–O8	91(1)	O7–P2–O6	106(1)		

separate trends exist for the dependence of cell volume and lattice parameters on the ionic radius of the tetravalent metal. Relative to their ionic radii group 4 materials have a larger a and b, and a smaller c parameter than group 14 materials. In the separate series, the cells increase approximately linearly with the radius of M. Thus, α-ZrP is not an anomaly.

One might speculate that the differences between the two series are caused by differences in the corresponding electronegativities. While the M–O bonds can be described as polar covalent for Ge, Sn and Pb (Pauling's electronegativity differences 1.34, 1.48, 1.64), they are increasingly ionic for Ti, Hf and Zr (differences 1.9, 2.14, 2.11). Therefore, a conceivable effect is that the oxygen ions in the group 14 containing *APTM* carry a lower real charge, allowing the **ab**-plane to contract and simultaneously leading to a stronger corrugation of the layers. This could possibly explain the observed increase of the interlayer distance and lattice parameter c.

3.2. Thermal behaviour of α-GeP from 300 to 16 K

The temperature dependence of the cell edges and the linear thermal expansion coefficients were obtained by Rietveld refinements of variable temperature diffraction data and described using the approach as given in e.g., [24]:

$$\alpha_i = \sum_{j=1}^{n} X_j \frac{(\theta_j/T)^2 \exp(\theta_j/T)}{[\exp(\theta_j/T)-1]^2}, \tag{1}$$

$$\ln\left(\frac{a_i}{a_{i,T_0}}\right) = \left[\sum_{j=1}^{n} \frac{X_j \theta_j}{\exp(\theta_j/T)-1}\right]_{T_0}^{T}, \tag{2}$$

where $\theta_j = h\nu_j/k_B$ is the mode frequency and X_j represents the effects of the mode Grüneisen parameter, bulk modulus, density of states, and volume. The temperature dependence of each lattice parameters could be well described by one θ_j mode. The temperature dependence of the monoclinic angle β was empirically parameterised in the form of a cosine term $\beta(T) = \beta_0 - A + A\cos(B \cdot T)$ (e.g., [25]), thus giving a physically acceptable behaviour of $\partial\beta/\partial T$ and consequently $\partial V/\partial T$ at $T = 0$ K. The corresponding refined parameters are given in Table 4. Fig. 5 shows the evolution of the normalised lattice parameters with temperature, and the resulting fits. As can be expected for a layered material with relatively weak interlayer interactions, α-GeP exhibits a significantly larger thermal expansion in the stacking direction of the layers in comparison with intra-layer expansion.

Using the parameters refined in the least squares fit of the variation of the lattice parameters with temperature, the temperature behaviour of the tensor of thermal expansion could be calculated. Since tensorial properties are defined in a Cartesian coordinate system with basic vectors $\mathbf{e}_i$, the Cartesian axes are not necessarily parallel to the crystallographic basic vectors. The Langrangian thermal expansion tensor coefficients for a monoclinic crystal with **b** as unique axis are given by

$$\alpha_{11}(T) = \frac{1}{a_0 \sin\beta_0}\left[\sin\beta \frac{da}{dT} + a\cos\beta \frac{d\beta}{dT}\right], \tag{3}$$

$$\alpha_{22}(T) = \frac{1}{b_0}\frac{db}{dT}, \tag{4}$$

$$\alpha_{33}(T) = \frac{1}{c_0}\frac{dc}{dT} \tag{5}$$

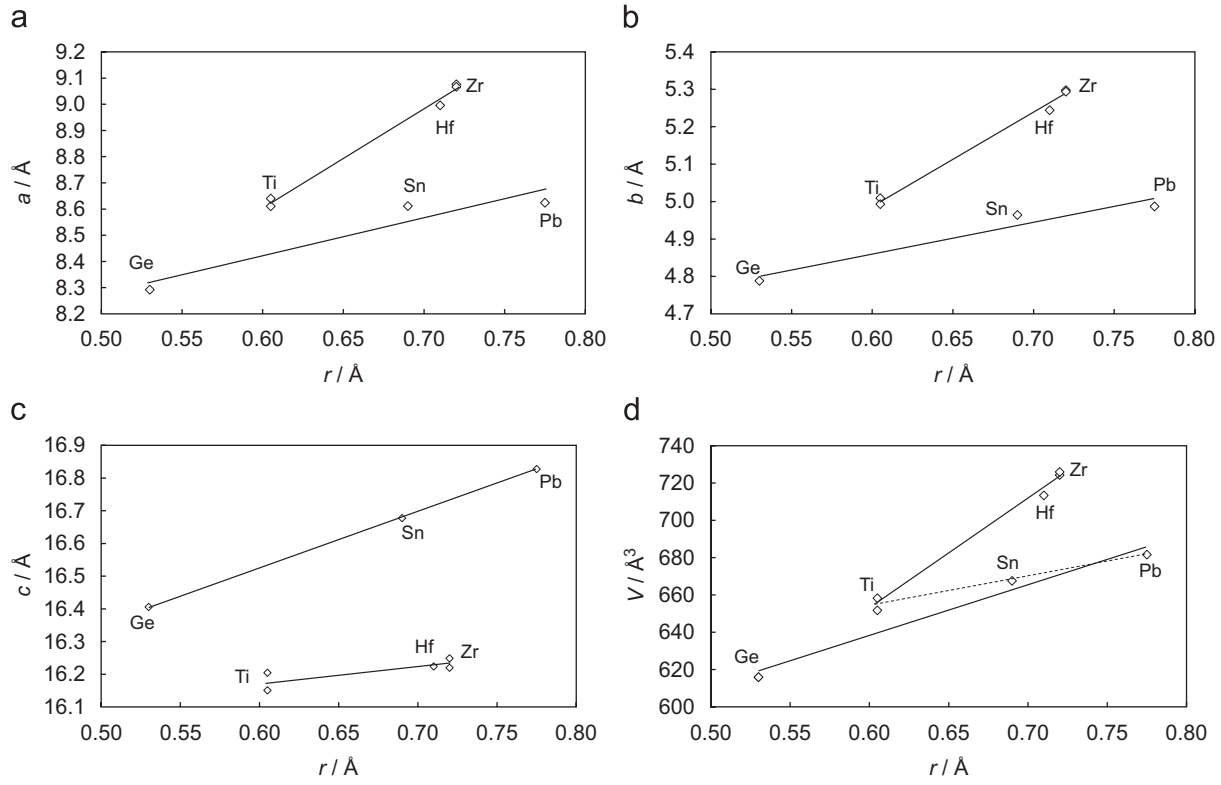

Fig. 4. Evolution of the lattice parameters a(a), b(b), c(c) and the cell volume (d) of *APTM* with α-ZrP type structure as a function of ionic radius [29] of the tetravalent metal. Solid lines are guides to the eye. The dashed line in (d) corresponds to the trend suggested by [15]. Data points are from this work (Ge), [15] (Ti, Sn, Zr, Pb), [14] (Zr), and [16] (Ti, Hf).

Table 4
Refined lattice parameters a_{i,T_0} ($i = 1, 2, 3 \equiv a, b, c$) and constants X_1 of α-GeP in the temperature range $16\,\mathrm{K} \leqslant T \leqslant 300\,\mathrm{K}$ for the θ_1 modes

i	a_{i,T_0}/Å	θ_1/K	$X_1 \times 10^5$ K
1	8.27101(4)	333(5)	1.28(1)
2	4.77451(3)	353(6)	1.52(2)
3	16.2963(3)	267(6)	3.54(4)

The refined parameters for β are: $\beta_0 = 109.126(3)^\circ$, $A = 8.3(1) \times 10^{-2}$ (°), $B = 4.30(6) \times 10^{-1}$ (° K^{-1}).

and

$$\alpha_{13}(T) = \frac{1}{a_0}\frac{\mathrm{d}a}{\mathrm{d}T}\left[\frac{1}{\sin 2\beta_0} - \frac{\sin\beta}{2\cos\beta_0}\right] - \frac{a\cos\beta}{2a_0\cos\beta_0}\frac{\mathrm{d}\beta}{\mathrm{d}T} - \frac{\cot\beta_0}{2c_0}\frac{\mathrm{d}c}{\mathrm{d}T}, \quad (6)$$

e.g., [26]. General expressions for the components of the linear and finite (Green's Strain) Langrangian and linear and finite (Almansi's) Eulerian strain tensors in terms of a crystal's lattice parameters before and after a deformation were derived by Schlenker et al. [27]. The $\mathrm{d}a_i/\mathrm{d}T$ in Eqs. (3)–(6) have been calculated from Eqs. (1)–(2) and the expression for β, using the coefficients and a_{i,T_0} quoted in Table 4. The principal components and their directions were calculated by the standard method of eigenvalue and eigenvector decomposition of the tensor [α]. In the present case, the principal axes lengths $\alpha_i\,(i = 1, 2, 3)$ are given by

$$\alpha_2 = \alpha_{22} \quad \text{and} \quad \alpha_1, \alpha_3 = \tfrac{1}{2}(\alpha_{11} + \alpha_{33} \pm \sqrt{D}), \quad (7)$$

where + and − correspond to α_1 and α_3, respectively. D is given by

$$D = (\alpha_{11} + \alpha_{33})^2 + 4(\alpha_{13}^2 - \alpha_{11}\alpha_{33}). \quad (8)$$

By symmetry, $\alpha_2 \parallel \mathbf{b}$. The direction of α_1 is $\perp$ to **b** and forms an angle θ with **c**:

$$\theta = \tan^{-1}\left(\frac{\alpha_{13}}{\alpha_1 - \alpha_{11}}\right). \quad (9)$$

See e.g., [28] for the analogous derivation of the general strain tensor components.

A strong anisotropy in thermal expansion can be observed for α-GeP. While the magnitudes for α_2 and α_3 reach values of $1.4 \times 10^{-5}\,\mathrm{K}^{-1}$ and $0.9 \times 10^{-5}\,\mathrm{K}^{-1}$ and do not appear to have reached saturation at 300 K, the magnitude for α_1 seems to saturate at a value of about $3.3 \times 10^{-5}\,\mathrm{K}^{-1}$ between 200 and 250 K, i.e., around 2−3 × larger (Fig. 6). This correlates with the determined θ_j given in Table 4. The orientation of the representation quadric (axes lengths are related to $1/\sqrt{\alpha_i}$) at 300 K with respect to the crystallographic coordinate system is shown in Fig. 7. Considering the monoclinic angle $\beta = 108.985(1)^\circ$, the determined angle $\theta \approx 25^\circ$ at room temperature leads to the direction of largest thermal expansion being almost

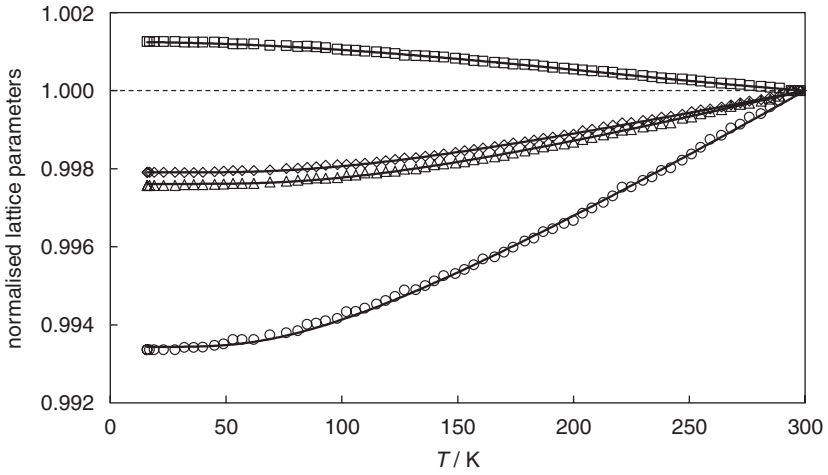

Fig. 5. Evolution of the normalised lattice parameters a (diamonds), b (triangles), c (circles), and β (squares) of α-GeP with temperature. Error bars are smaller than the symbols used. Lines correspond to fits using the equations stated in the text and the values for the coefficients as given in Table 4.

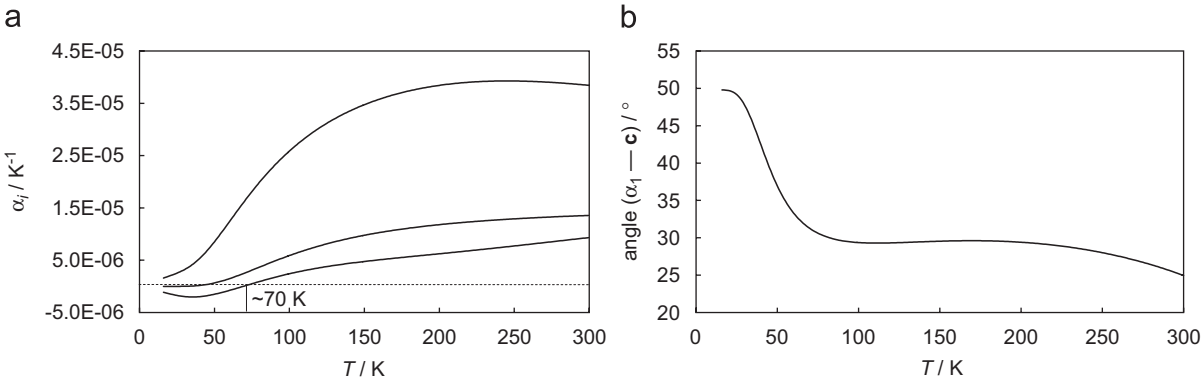

Fig. 6. Temperature dependence of the magnitudes of the thermal expansion tensor's principal axes (a): α_1 (upper line), α_2 (middle line) and α_3 (bottom line), and the orientation angle θ between α_1 and **c** (b).

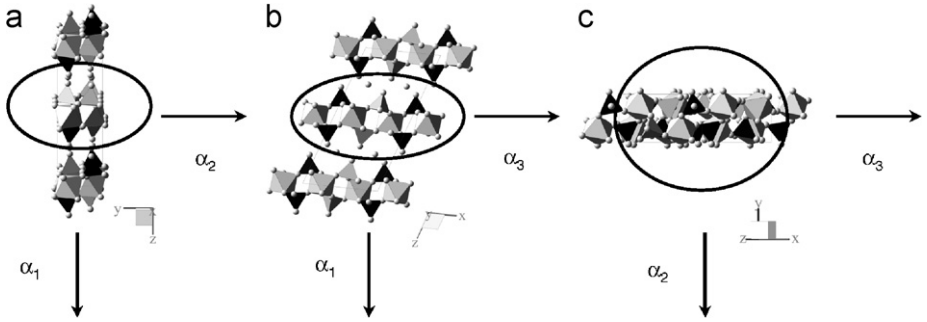

Fig. 7. Orientation of the representation quadric of the thermal expansion in α-GeP with respect to the crystallographic axes at 300 K. (a–c) correspond to views along the principal axes. Axes lengths are proportional to $1/\sqrt{\alpha_i}$.

perpendicular (84°) to the **ab**-plane. Thus, the thermal behaviour of α-GeP is dominated by the increasing interlayer distance with increasing temperature.

At low temperatures (≈ 70 K), the representation surface of the tensor changes its shape from an ellipsoid towards a hyperboloid of one sheet, due to a change in the sign of α_3. However, we cannot exclude that this observation, as well as the rapid change in the orientation of α_1 with respect to **c** in the same temperature regime, is caused by the fact that thermal expansion necessarily approaches zero at low temperature, and thus both axes lengths and orientation of the quadric become less well defined.

The X-ray data used to extract the cell parameters reported in Fig. 5 are not of sufficient quality to obtain

reliable information on changes in oxygen coordinates with temperature. We therefore cannot comment on minor internal structural changes in α-GeP which may occur as a function of temperature.

4. Summary and conclusions

The crystal structure of α-GeP has been redetermined in this work. Its lattice parameters at room temperature are $a = 8.2916(2)$ Å, $b = 4.7880(1)$ Å, $c = 16.4063(3)$ Å and $\beta = 108.987(1)^\circ$ in space group $P2_1/c$. It has been confirmed that α-GeP has α-ZrP type structure. An interpretation for the observed geometrical trends in *APTM* with α-ZrP type structure has been suggested. The thermal behaviour of the title compound has been studied from 300 to 16 K. No structural phase transitions have been observed. The variation of the thermal expansion tensor's principal axes lengths and their orientation towards the crystallographic basic vectors with temperature have been derived. Thermal expansion in **c** direction exceeds those of the other cell edges by a factor of 2–3, thus the main structural mechanism for the expansion is the increase of the interlayer gap with increasing temperature.

Acknowledgment

Financial support by the Engineering and Physical Science Research Council EPSRC (EP/C538927/1) is gratefully acknowledged.

References

[1] A. Clearfield, J.A. Stynes, The preparation of crystalline zirconium phosphate and some observations on its ion exchange behaviour, J. Inorg. Nucl. Chem. 26 (1964) 117–129.
[2] A. Clearfield, R.H. Blessing, J.A. Stynes, New crystalline phases of zirconium phosphate possessing ion-exchange properties, J. Inorg. Nucl. Chem. 30 (1968) 2249–2258.
[3] A. Clearfield, (Ed.), Inorganic Ion Exchange Materials, CRC Press, Boca Raton, Florida, USA, 1982.
[4] T. Kijima, Y. Matsui, A new type of host compound consisting of α-zirconium phosphate and an animated cyclodextrin, Nature 322 (1986) 533–534.
[5] A. Clearfield, Structural concepts in inorganic proton conductors, Solid State Ion. 46 (1991) 35–43.
[6] A. Guerrero-Ruiz, I. Rodríguez-Ramos, J.L. García-Fierro, A. Jiménez-López, P. Olivera-Pastor, P. Maireles-Torres, Catalytic activity of layered α-(tin or zirconium) phosphates and chromia-pillared derivatives for isopropyl alcohol decomposition, Appl. Catal. A 92 (1992) 81–92.
[7] E.R. Losilla, A. Cabeza, S. Bruque, M.A.G. Aranda, J. Sanz, J.E. Iglesias, J.A. Alonso, Syntheses, structures, and thermal expansion of germanium pyrophosphates, J. Solid State Chem. 156 (2001) 213–219.
[8] J.S.O. Evans, Negative thermal expansion materials, J. Chem. Soc. Dalton Trans. (1999) 3317–3326.
[9] V. Korthuis, N. Khosrovani, A.W. Sleight, N. Roberts, R. Dupree, W.W. Warren Jr., Negative thermal expansion and phase transitions in the $ZrV_{2-x}P_xO_7$ Series, Chem. Mater. 7 (1995) 412–417.
[10] A. La Ginestra, P. Galli, M.L. Berardelli, Thermal behaviour of germanium bis(monohydrogenphosphate) monohydrate and characterization of derived germanium pyrophosphates, J. Chem. Soc. Dalton Trans. 4 (1984) 527–531.
[11] R. Romano, A.I. Ruiz, O.L. Alves, Multiple-step preparation and physicochemical characterization of crystalline α-germanium hydrogenphosphate, J. Solid State Chem. 177 (2004) 1520–1528.
[12] A.P.A. Moraes, R. Romano, A.G. Souza Filho, P.T.C. Freire, J. Mendes Filho, O.L. Alves, Vibrational spectra of α-$Ge(HPO_4)_2 \cdot H_2O$ compound, Vib. Spectrosc. 40 (2006) 209–212.
[13] A. Winkler, E. Thilo, Über eine Reihe saurer Verbindungen $HX^VP_2O_8$ und $H_2X^{IV}P_2O_8$ mit Schichtstruktur, X^V = As und Sb; X^{IV} = Si, Ge, Sn, Pb, Ti, Zr, Z. Anorg. Allg. Chem. 346 (1966) 91–112.
[14] A. Clearfield, G.D. Smith, The crystallography and structure of α-zirconium bis(monohydrogen orthophosphate) monohydrate, Inorg. Chem. 8 (1969) 431–436.
[15] S. Bruque, M.A.G. Aranda, E.R. Losilla, P. Olivera-Pastor, P. Maireles-Torres, Synthesis optimization and crystal structures of layered metal(IV) hydrogen phosphates, α-$M(HPO_4)_2 \cdot H_2O$ (M = Ti, Sn, Pb), Inorg. Chem. 34 (1995) 893–899.
[16] M.A. Salvadó, P. Pertierra, S. García-Granda, J.R. García, J. Rodríguez, M.T. Fernández-Díaz, Neutron powder diffraction study of α-$Ti(HPO_4)_2 \cdot H_2O$ and α-$Hf(HPO_4)_2 \cdot H_2O$; H-atom positions, Acta Crystallogr. B 52 (1996) 896–898.
[17] A.N. Christensen, E. Krogh-Andersen, I.G. Krogh-Andersen, G. Alberti, M. Nielsen, M.S. Lehmann, X-ray powder diffraction study of layer compounds. The crystal structure of α-$Ti(HPO_4)_2 \cdot H_2O$ and a proposed structure for γ-$Ti(HPO_4)_2 \cdot H_2O$, Acta Chem. Scand. 44 (1990) 865–872.
[18] J.M. Troup, A. Clearfield, On the mechanism of ion exchange in zirconium phosphates. 20. Refinement of the crystal structure of α-zirconium phosphate, Inorg. Chem. 16 (1977) 3311–3314.
[19] G.S. Pawley, Unit cell refinement from powder diffraction scans, J. Appl. Crystallogr. 14 (1981) 357–361.
[20] H. Rietveld, Line profiles of neutron powder-diffraction peaks for structure refinements, Acta Crystallogr. 22 (1967) 151–152.
[21] A.A. Coelho, TOPAS v2.0: General Profile and Structure Analysis Software for Powder Diffraction Data, 2000.
[22] W.A. Dollase, Correction of intensities for preferred orientation in powder diffractometry: application of the March model, J. Appl. Crystallogr. 19 (1986) 267–272.
[23] A.A. Coelho, Indexing of powder diffraction patterns by iterative use of singular value decomposition, J. Appl. Crystallogr. 36 (2003) 86–95.
[24] K. Wang, R.R. Reeber, Mode Grüneisen parameters and negative thermal expansion of cubic ZrW_2O_8 and $ZrMo_2O_8$, Appl. Phys. Lett. 76 (2000) 2203–2204.
[25] K.S. Knight, I.C. Stretton, P.F. Schofield, Temperature evolution between 50 and 320 K of the thermal expansion tensor of gypsum derived from neutron powder diffraction data, Phys. Chem. Miner. 26 (1999) 477–483.
[26] J.L. Schlenker, G.V. Gibbs, M.B. Boisen, Thermal expansion coefficients for monoclinic crystals: a phenomenological approach, Am. Mineral. 81 (1975) 823–833.
[27] J.L. Schlenker, G.V. Gibbs, M.B. Boisen, Strain-tensor components expressed in terms of lattice parameters, Acta Crystallogr. A 34 (1978) 52–54.
[28] Y. Ohashi, C.W. Burnham, Clinopyroxene lattice deformations: the roles of chemical substitution and temperature, Am. Mineral. 58 (1973) 843–849.
[29] R.D. Shannon, Revised effective ionic radii and systematic studies of interatomic distances in halides and chalcogenides, Acta Crystallogr. A 32 (1976) 751–767.